

# Precision Determination of the Neutron Spin Structure Function $g_1^n$

K. Abe<sup>21</sup>, T. Akagi<sup>18,21</sup>, B. D. Anderson<sup>7</sup>, P. L. Anthony<sup>18</sup>, R. G. Arnold<sup>1</sup>, T. Averett<sup>5</sup>, H. R. Band<sup>23</sup>, C. M. Berisso<sup>9</sup>, P. Bogorad<sup>15</sup>, H. Borel<sup>6</sup>, P. E. Bosted<sup>1</sup>, V. Breton<sup>3</sup>, M. J. Buenerd<sup>18</sup>, G. D. Cates<sup>15</sup>, T. E. Chupp<sup>10</sup>, S. Churchwell<sup>9</sup>, K. P. Coulter<sup>10</sup>, M. Daoudi<sup>18</sup>, P. Decowski<sup>17</sup>, R. Erickson<sup>18</sup>, J. N. Fellbaum<sup>1</sup>, H. Fonvieille<sup>3</sup>, R. Gearhart<sup>18</sup>, V. Ghazikhanian<sup>8</sup>, K. A. Griffioen<sup>22</sup>, R. S. Hicks<sup>9</sup>, R. Holmes<sup>19</sup>, E. W. Hughes<sup>5</sup>, G. Igo<sup>8</sup>, S. Incerti<sup>3</sup>, J. R. Johnson<sup>23</sup>, W. Kahl<sup>19</sup>, M. Khayat<sup>7</sup>, Yu. G. Kolomensky<sup>9</sup>, S. E. Kuhn<sup>13</sup>, K. Kumar<sup>15</sup>, M. Kuriki<sup>21</sup>, R. Lombard-Nelsen<sup>6</sup>, D. M. Manley<sup>7</sup>, J. Marroncle<sup>6</sup>, T. Maruyama<sup>18</sup>, T. Marvin<sup>16</sup>, W. Meyer<sup>4</sup>, Z.-E. Meziani<sup>20</sup>, D. Miller<sup>12</sup>, G. Mitchell<sup>23</sup>, M. Olson<sup>7</sup>, G. A. Peterson<sup>9</sup>, G. G. Petratos<sup>7</sup>, R. Pitthan<sup>18</sup>, R. Prepost<sup>23</sup>, P. Raines<sup>14</sup>, B. Raue<sup>13</sup>, D. Reyna<sup>1</sup>, L. S. Rochester<sup>18</sup>, S. E. Rock<sup>1</sup>, M. V. Romalis<sup>15</sup>, F. Sabatie<sup>6</sup>, G. Shapiro<sup>2</sup>, J. Shaw<sup>9</sup>, T. B. Smith<sup>10</sup>, L. Sorrell<sup>1</sup>, P. A. Souder<sup>19</sup>, F. Staley<sup>6</sup>, S. St. Lorant<sup>18</sup>, L. M. Stuart<sup>18</sup>, F. Suekane<sup>21</sup>, Z. M. Szalata<sup>1</sup>, Y. Terrien<sup>6</sup>, A. K. Thompson<sup>11</sup>, T. Toole<sup>1</sup>, X. Wang<sup>19</sup>, J. W. Watson<sup>7</sup>, R. C. Welsh<sup>10</sup>, F. Wesselmann<sup>13</sup>, T. Wright<sup>23</sup>, C. C. Young<sup>18</sup>, B. Youngman<sup>18</sup>, H. Yuta<sup>21</sup>, W.-M. Zhang<sup>7</sup>, and P. Zyla<sup>20</sup>

<sup>1</sup> American University, Washington, DC 20016

<sup>2</sup> University of California, Berkeley, CA 94720

<sup>3</sup> LPC IN2P3/CNRS, Univ. Blaise Pascal, F-63170 Aubiere Cedex, France

<sup>4</sup> University of Bonn, Nussallee 12 D-5300 Bonn, Germany

<sup>5</sup> California Institute of Technology, Pasadena, California 91125

<sup>6</sup> DAPNIA, Saclay, 91191 Gif-sur-Yvette Cedex, France

<sup>7</sup> Kent State University, Kent, OH 44242

<sup>8</sup> University of California, Los Angeles, CA 90024-1547

<sup>9</sup> University of Massachusetts, Amherst, MA 01003

<sup>10</sup> University of Michigan, Ann Arbor, MI 48109

<sup>11</sup> National Institute of Standards and Technology, Gaithersburg, MD 20899

<sup>12</sup> Northwestern University, Evanston, IL 60201

<sup>13</sup> Old Dominion University, Norfolk, VA 23529

<sup>14</sup> University of Pennsylvania, Philadelphia, PA 19104-6317

<sup>15</sup> Princeton University, Princeton, NJ 08544

<sup>16</sup> Southern Oregon State College, Ashland, OR 97520

<sup>17</sup> Smith College, Northampton, MA 01063

<sup>18</sup> Stanford Linear Accelerator Center, Stanford, CA 94309

<sup>19</sup> Syracuse University, Syracuse, NY 13210

<sup>20</sup> Temple University, Philadelphia, PA 19122

<sup>21</sup> Tohoku University, Aramaki Aza Aoba, Sendai, Miyagi, Japan

<sup>22</sup> College of William and Mary, Williamsburg, VA 23187

<sup>23</sup> University of Wisconsin, Madison, WI 53706

(E154 Collaboration)

We report on a precision measurement of the neutron spin structure function  $g_1^n$  using deep inelastic scattering of polarized electrons by polarized  $^3\text{He}$ . For the kinematic range  $0.014 < x < 0.7$  and  $1 \text{ (GeV/c)}^2 < Q^2 < 17 \text{ (GeV/c)}^2$ , we obtain  $\int_{0.014}^{0.7} g_1^n(x) dx = -0.036 \pm 0.004 \text{ (stat)} \pm 0.005 \text{ (syst)}$  at an average  $Q^2 = 5 \text{ (GeV/c)}^2$ . We find relatively large negative values for  $g_1^n$  at low  $x$ . The results call into question the usual Regge theory method for extrapolating to  $x=0$  to find the full neutron integral  $\int_0^1 g_1^n(x) dx$ , needed for testing quark-parton model and QCD sum rules.

Deep inelastic scattering (DIS) of polarized leptons by polarized nucleons has been the cornerstone for studying the internal spin structure of the proton and neutron. Although the first experiments [1,2] found large asymmetries in the spin-dependent scattering of electrons by protons, consistent with the early quark-parton model (QPM) predictions [3], subsequent experiments [4-6] performed at higher energies found that the proton asymmetries at low values of Bjorken  $x$  disagreed with the early QPM predictions. In fact, higher energy proton measurements were inconsistent with one of the QPM sum rules

derived by Ellis and Jaffe [7] based upon an unpolarized strange sea. First measurements of spin-dependent scattering of polarized leptons off polarized neutrons found small negative asymmetries, and, along with the proton results, provided the first tests of the fundamental Bjorken Sum Rule [8]. However, the neutron results suffered either from large statistical uncertainties at low  $x$  [9,10], or from a limited beam energy [11,12]. This Letter reports on a precision measurement of the neutron spin structure function  $g_1^n$  performed at the Stanford Linear Accelerator Center (SLAC) using 48.3 GeV polarized

electrons scattered from polarized  $^3\text{He}$  to achieve  $x$  values as low as 0.014. The present experiment (E154), which collected  $10^8$  events in October and November of 1995, builds on the experience from the previous SLAC  $^3\text{He}$  experiment (E142) [11] performed at a lower beam energy. The E154 results provide a new insight into the low  $x$

behavior of  $g_1^n$ .

The asymmetries  $A_{\parallel}(A_{\perp})$  measured in DIS of longitudinally polarized electrons by longitudinally (transversely) polarized nucleons can be used to find the nucleon spin structure function  $g_1$  [13], namely

$$g_1(x, Q^2) = F_2(x, Q^2) \frac{1 + \gamma^2}{2xD'(1 + R(x, Q^2))} [A_{\parallel} + \tan(\theta/2)A_{\perp}],$$

where  $Q^2$  is the squared four-momentum transfer of the virtual photon;  $x$  is the fraction of nucleon momentum carried by the struck quark;  $\gamma$  and  $D'$  are factors depending on the scattered electron's initial and final energies and the electron scattering angle  $\theta$ ;  $F_2(x, Q^2)$  is the unpolarized nucleon spin structure function and  $R(x, Q^2) = \sigma_L/\sigma_T$  is the longitudinal to transverse virtual photoabsorption cross section ratio. The asymmetries  $A_{\parallel}(A_{\perp})$  may also be used to find the virtual photon-nucleon asymmetries  $A_1(x, Q^2)$ .

Polarized electrons were obtained using a strained GaAs cathode illuminated by circularly polarized light from a flashlamp-pumped Ti:sapphire laser [14]. The electron spin direction was reversed randomly on a pulse-to-pulse basis by reversing the helicity of the laser light. The electrons were subsequently accelerated to 48.3 GeV and directed to the experimental hall. The charge per pulse ranged from 3 to  $9 \times 10^{10}$  electrons, yielding an average current ranging from 0.5 to 2  $\mu\text{A}$  for a pulse repetition rate of 120 Hz and a pulse width of 250 ns. The beam polarization was measured to be  $0.82 \pm 0.02$  over the duration of the experiment using a single arm Møller polarimeter [15] located upstream of the target.

The polarized  $^3\text{He}$  target consisted of double-chamber glass cells [16] filled with  $\sim 9.5$  atm of  $^3\text{He}$  (as measured at  $20^\circ\text{C}$ ). The 30 cm long cells were constructed of Corning 1720 glass. The lower chamber had  $\sim 50 \mu\text{m}$  inverted end windows through which the electron beam passed. Approximately 50 torr of nitrogen gas was also present in the cells to aid in optical pumping. The  $^3\text{He}$  nuclei were polarized in the upper chamber by spin-exchange collisions with optically-pumped polarized rubidium atoms [17,18]. Three 20 W diode lasers and four Argon-ion pumped Ti:sapphire lasers continuously polarized the rubidium atoms in the upper chamber of the target cell. The target spin direction was reversed approximately once a week throughout the experiment. NMR techniques [19] calibrated by proton NMR and by frequency shift techniques [20], were used to measure the polarization of the  $^3\text{He}$  nuclei. The polarization ranged as high as 0.48 and was on average  $0.38 \pm 0.02$  over the duration of the experiment. The systematic uncertainty in the target polarization was dominated by the water calibration for the NMR technique and by uncertainties in the polarization gradients

and  $^3\text{He}$  density for the frequency shift technique.

Two new single-arm spectrometers, at central scattering angles of  $2.75^\circ$  and  $5.5^\circ$ , were used to analyze scattered electrons [21]. Each spectrometer utilized a pair of threshold Čerenkov counters operating with nitrogen at a pressure of 0.10 (0.14) atm in the  $2.75^\circ$  ( $5.5^\circ$ ) arm, corresponding to a pion energy threshold of approximately 19 (16) GeV. Ten (eight) planes of hodoscopes were used for tracking in the  $2.75^\circ$  ( $5.5^\circ$ ) spectrometer. Tracking resolution resulted in a momentum determination ranging from  $\pm 2\%$  at low momentum to  $\pm 4\%$  at high momentum. The momentum resolution was useful for reducing the contamination from hadronic backgrounds to the electron sample. At the rear of each spectrometer a 200 block lead glass calorimeter was arranged in a fly's eye configuration [22] which gave an energy resolution of  $3\% + (8/\sqrt{E(\text{GeV})})\%$ . Only events with scattered electron energies greater than 10 GeV were used in the analysis, corresponding to  $Q^2 > 1 (\text{GeV}/c)^2$  for the  $2.75^\circ$  spectrometer.

For each beam pulse, the experiment collected information from the hodoscope and calorimeter multihit TDCs and the calorimeter ADCs. The four Čerenkov counters were each read out by a Flash ADC that recorded the pulse shape in 1 ns time slices covering the full beam pulse. Events were analyzed as electron candidates if they passed a low-threshold in both Čerenkov counters in coincidence with an energy cluster in the lead glass. Events were tracked using the lead glass centroid cluster position and hits in the hodoscope planes. The tracks, combined with information on the spectrometer optics, were used to determine the particle's momentum. Tracking efficiency was measured to be on the order of 90%. Events were also classified by the energy deposition in the calorimeter. When the ratio of the energy deposited in the calorimeter to the momentum determined from tracking for an event was less than 80%, the event was rejected as a pion candidate. Typically 0.5 (0.2) electrons and 5 (2) pions were recorded per pulse in the  $2.75^\circ$  ( $5.5^\circ$ ) spectrometer. Selected events were binned in  $x$  and tagged per pulse with the relative beam and target spin directions.

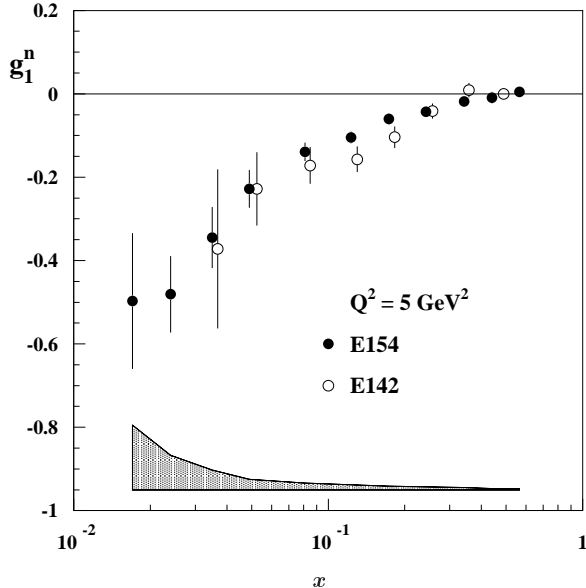


FIG. 1. Results for  $g_1^n$  versus  $x$  from SLAC Experiment E154 compared to Experiment E142 evaluated at  $Q^2 = 5$   $(\text{GeV}/c)^2$ . Shaded region corresponds to  $1 \sigma$  systematic uncertainties.

Contamination of hadronic background in the electron sample was measured to be  $3 \pm 2 \%$  for the lowest  $x$  values and decreased at higher values. Furthermore, since the hadron asymmetries were found to be approximately  $1/3$  the size of the electron asymmetries, the total effect of hadron contamination was very small. On the other hand, a relatively large contamination of the DIS electron sample originates from electrons produced from charge-symmetric decays of hadrons. The rates from this background were determined from running with the spectrometer polarity reversed to measure positrons. The rates for the non-DIS electron event background were on the order of  $15\%$  at the lowest scattered electron energies and fell rapidly with increasing energy. The measured asymmetries from these runs were found to be consistent with zero.

The fraction of DIS events that come from polarized  $^3\text{He}$  as compared to the full target cell is called the dilution factor. It was determined from known unpolarized nucleon structure functions, measured glass cell window thicknesses and the density of gas in the target cells (material method). The dilution factor was also determined by comparing rates from the polarized target to rates from a dummy cell with different gas pressures (rate method). This method has the advantage of taking into account possible beam halo effects. Results were obtained using the material method, and the rate procedure was used to assign systematic uncertainties. On average, the dilution factor was found to be  $0.55 \pm 0.03$ .

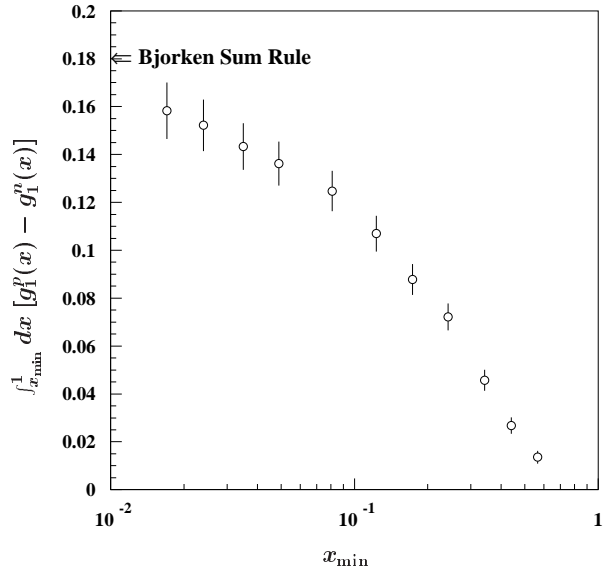


FIG. 2. Difference between the measured proton [5,6] and neutron [This experiment] integrals calculated from a minimum  $x$  value,  $x_{\min}$  up to  $x$  of 1. The value is compared to the theoretical prediction from the Bjorken sum rule which makes a prediction over the full  $x$  range. For the prediction, the Bjorken sum rule is evaluated up to third order in  $\alpha_s$  [23,24] and at  $Q^2 = 5$   $(\text{GeV}/c)^2$ . Error bars on the data are dominated by systematic uncertainties and are highly correlated point-to-point.

After corrections for hadronic and pair-symmetric backgrounds, dilutions and polarizations, the asymmetries  $A_{\parallel}$  and  $A_{\perp}$  were formed. The asymmetries were corrected for radiative processes to find the single-photon exchange Born results [25–28]. Uncertainties in the radiative corrections were estimated by varying the input models over a range consistent with the measured data.

Corrections due to the nuclear wave function of the polarized  $^3\text{He}$  nucleus were applied [29–32] using the recent proton data [5,6] to evaluate the proton contributions; however these contributions had only a small impact on the results. No other corrections were made for the fact that the polarized neutron is embedded in the  $^3\text{He}$  nucleus.

Results for  $A_1^n$  and  $g_1^n$  are presented in Table 1, and  $g_1^n$  is plotted in Fig. 1 along with the results of the SLAC E142 experiment [11]. The results from both experiments are evolved to  $Q^2 = 5$   $(\text{GeV}/c)^2$  under the assumption that  $g_1/F_1$  is independent of  $Q^2$ . Within experimental uncertainties, this assumption is supported by a comparison of our data to all existing measurements [9–12,33,34]. Good agreement with the E142 results is seen in the overlapping  $x$  range. Over the range of this experiment, we find a neutron spin structure function integral of  $\int_{0.014}^{0.7} g_1^n(x) dx = -0.036 \pm 0.004$  (stat.)  $\pm 0.005$  (syst.).

A notable feature of Fig. 1 is the strong  $x$ -dependence observed at low  $x$ , a result that is incompatible with the

simplest Regge theory interpretation [35,36] that  $g_1^n$  is constant with  $x$  in this region. The strong  $x$ -dependence also implies that the unmeasured small- $x$  region can make a major contribution to the integral  $\int_0^1 g_1^n(x)dx$  and recourse must be made to models in order to evaluate the full integral. The result is that the value extracted for the integral is subject to considerable model uncertainty. For example, a Regge theory extrapolation with functional form  $g_1^n \sim x^{-\alpha}$ ,  $-0.5 < \alpha \leq 0$ , yields  $\int_0^1 g_1^n(x)dx = -0.041 \pm 0.004 \pm 0.006$ , even though this description is successful in fitting only the three lowest  $x$  points at  $x < 0.04$ . In contrast, a fit to the  $x < 0.1$  data with an unconstrained power-law yields  $\int_0^1 g_1^n(x)dx = -0.2$ . No uncertainty can be given for this later analysis, since the fitted value of  $\alpha$  is  $0.9 \pm 0.2$ , and the integral diverges for  $\alpha = 1$ . Figure 3 summarizes the results of the fits described above to the low  $x$  data region. If we fit an unconstrained power law to the measured  $g_1^n$  values without evolving to  $Q^2 = 5 \text{ GeV}^2$ , we find  $\alpha$  is  $0.7 \pm 0.2$ . In short, the new data do not adequately constrain the low- $x$  region such that the integral of  $g_1^n$  can be reliably extracted.

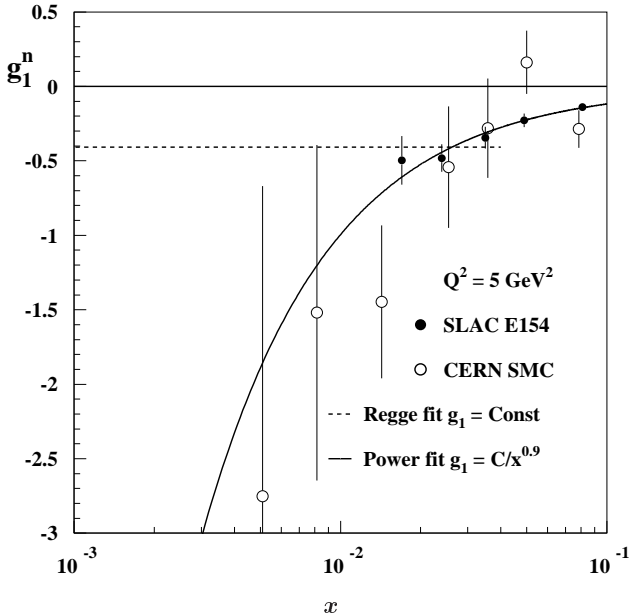


FIG. 3. Results for  $g_1^n$  versus  $x$  for the low  $x$  region from SLAC experiment E154 compared to the CERN SMC experiment. The data is evolved to  $Q^2 = 5 \text{ (GeV}^2/c^2)$ . Fits that impact the low  $x$  extrapolation (discussed in the text) are presented.

We have also used the present precision neutron results down to  $x_{\min} = 0.014$  along with the proton results from SLAC E143 experiment ( $0.03 < x$ ) [6] and the CERN SMC experiment ( $0.014 < x < 0.03$ ) [5] to compare to the Bjorken sum rule prediction. The difference between proton and neutron spin structure functions integrated over  $x$  from  $x_{\min}$  to  $x=1$  is shown in Fig. 2. One sees

that the difference in the integral of  $g_1$  for the proton and neutron falls only 1.9 standard deviations below the Bjorken sum rule prediction when the data is integrated down to  $x$  of 0.014. Presumably the rest of the integral comes from the remaining unmeasured low  $x$  region.

In conclusion, we have found relatively large negative values of  $g_1^n$  at low  $x$ . One possible explanation for this behavior can be associated with sea and gluon spin contributions [37–39]. A breakdown in the simple Regge theory description at low  $x$  is also a possible consequence. Further precision data using proton and deuteron targets over the same kinematic range are expected to be of great use in unraveling the behavior of the nucleon spin structure functions at moderately low  $x$  (down to  $x \approx 0.01$ ). High precision low  $x$  measurements of the nucleon spin structure functions are still needed to understand how  $g_1^n$  converges at low  $x$  and to extract the neutron integral  $\int_0^1 g_1^n(x)dx$ .

We thank the personnel of the SLAC accelerator department for their efforts which resulted in the successful operation of the E154 Experiment. This work was supported by the Department of Energy; by the National Science Foundation; by the Kent State University Research Council (GGP); by the Jeffress Memorial Trust (KAG); by the Centre National de la Recherche Scientifique and the Commissariat à l’Energie Atomique (French groups); and by the Japanese Ministry of Education, Science and Culture (Tohoku).

- 
- [1] M. J. Alguard *et al.*, Phys. Rev. Lett. **37**, 1258 (1976); **37**, 1261 (1976).
  - [2] G. Baum *et al.*, Phys. Rev. Lett. **51**, 1135 (1983).
  - [3] R. D. Carlitz and J. Kaur, Phys. Rev. Lett. **37**, 673 (1977).
  - [4] J. Ashman *et al.*, Phys. Rev. Lett. **B206**, 364 (1988); Nucl. Phys. **B328**, 1 (1989).
  - [5] D. Adams *et al.*, Phys. Lett. **B329**, 399 (1994).
  - [6] K. Abe *et al.*, Phys. Rev. Lett. **74**, 346 (1995).
  - [7] J. Ellis and R. L. Jaffe, Phys. Rev. **D9**, 1444 (1974); **D10**, 1669 (1974).
  - [8] J. D. Bjorken, Phys. Rev. **148**, 1467 (1966); Phys. Rev. **D1**, 1376 (1970).
  - [9] D. Adams *et al.*, Phys. Lett. **B357**, 248 (1995).
  - [10] D. Adams *et al.*, Phys. Lett. **B396**, 338 (1997).
  - [11] P. L. Anthony *et al.*, Phys. Rev. Lett. **71**, 959 (1993); Phys. Rev. **D54**, 6620 (1996).
  - [12] K. Abe *et al.*, Phys. Rev. Lett. **75**, 25 (1995).
  - [13] See reference 11 for Phys. Rev. D. article for definitions of kinematic factors and unpolarized structure functions.
  - [14] T. Maruyama *et al.*, Phys. Rev. **B46**, 4261 (1992); R. Alley *et al.*, Report No. SLAC-PUB-6489, 1994.
  - [15] H. Band *et al.*, SLAC-PUB-7370 (1997), submitted to Nucl. Instr. Methods.

- [16] T. E. Chupp *et al.*, Phys. Rev. **C45**, 915 (1992).  
[17] M. A. Bouchiat, T. R. Carver and C. M. Varnum, Phys. Rev. Lett. **49**, 25 (1960).  
[18] T. E. Chupp *et al.*, Phys. Rev. **C36**, 2244 (1987).  
[19] A. Abragam, Principles of Nuclear Magnetism (Oxford University Press, New York, 1961).  
[20] N. R. Newbury *et al.*, Phys. Rev. **A48**, 558 (1993); A. S. Barton *et al.*, Phys. Rev. **A49**, 2766 (1994).  
[21] Yu. G. Kolomensky, PhD thesis, University of Massachusetts (February 1997).  
[22] H. Borel *et al.*, IEEE Trans. Nucl. Sci., **Vol. 42, No. 4**, 529 (1995) and Erratum, IEEE Trans. on Nucl. Sci, **Vol. 42, No. 6**, 8347 (1995).  
[23] S. A. Larin and J. A. M. Vermaseren, Phys. Lett. **B172**, 109 (1986).  
[24] Particle Data Group, R.M. Barnett *et al.*, Phys. Rev. **D53**, 6100 (1996).  
[25] T. V. Kuchto and N. M. Shumeiko, Nucl. Phys. **B219**, 412 (1983).  
[26] I. V. Akushevich and N. M. Shumeiko, J. Phys. G: Nucl. Part. Phys. **20**, 513 (1994).  
[27] L. W. Mo and Y. S. Tsai, Rev. Mod. Phys. **41**, 205 (1969).  
[28] Y. S. Tsai, Report No. SLAC-PUB-848 (1971).  
[29] C. Ciofi degli Atti *et al.*, Phys. Rev. **C48**, 968 (1993).  
[30] B. Blankleider and R. M. Woloshyn, Phys. Rev. **C29**, 538 (1984).  
[31] J. L. Friar *et al.*, Phys. Rev. **C42**, 2310 (1990).  
[32] R.-W. Shulze and P. U. Sauer, Phys. Rev. **C48**, 38 (1993).  
[33] K. Abe *et al.*, Phys. Lett. **B364**, 61 (1995).  
[34] K. Ackerstaff *et al.*, hep-ex/9703005 (1997), submitted to Phys. Lett..  
[35] R. L. Heinmann, Nucl. Phys. **B64**, 429 (1973).  
[36] J. Ellis and M. Karliner, Phys. Lett. **B213**, 73 (1988).  
[37] R. D. Ball, S. Forte and G. Ridolfi, Phys. Lett. **B378**, 255 (1996).  
[38] M. Gluck *et al.*, Phys. Rev. **D53**, 4775 (1996).  
[39] T. Gehrmann and W. J. Stirling, Phys. Rev. **D53**, 6100 (1996).

TABLE I. Results on  $A_1^n$  and  $g_1^n$  at the measured  $Q^2$ , along with  $g_1^n$  evaluated at  $Q^2 = 5$  (GeV/c) $^2$  assuming that  $g_1^n/F_1^n$  is independent of  $Q^2$ .

$x$ range	$\langle x \rangle$	$\langle Q^2 \rangle$ (GeV/c) $^2$	$g_1^n \pm \text{stat.} \pm \text{syst.}$	$A_1^n \pm \text{stat.} \pm \text{syst.}$	$g_1^n \pm \text{stat.} \pm \text{syst.}$ ( $Q^2 = 5$ (GeV/c) $^2$ )
0.014 – 0.02	0.017	1.2	$-0.351 \pm 0.115 \pm 0.110$	$-0.058 \pm 0.019 \pm 0.018$	$-0.497 \pm 0.163 \pm 0.155$
0.02 – 0.03	0.024	1.6	$-0.374 \pm 0.071 \pm 0.065$	$-0.080 \pm 0.015 \pm 0.014$	$-0.481 \pm 0.092 \pm 0.083$
0.03 – 0.04	0.035	2.0	$-0.290 \pm 0.061 \pm 0.039$	$-0.078 \pm 0.018 \pm 0.011$	$-0.345 \pm 0.073 \pm 0.047$
0.04 – 0.06	0.049	2.6	$-0.204 \pm 0.040 \pm 0.022$	$-0.086 \pm 0.016 \pm 0.010$	$-0.228 \pm 0.045 \pm 0.025$
0.06 – 0.10	0.081	4.4	$-0.137 \pm 0.021 \pm 0.016$	$-0.092 \pm 0.013 \pm 0.011$	$-0.139 \pm 0.022 \pm 0.016$
0.10 – 0.15	0.123	6.6	$-0.108 \pm 0.015 \pm 0.012$	$-0.106 \pm 0.014 \pm 0.012$	$-0.105 \pm 0.014 \pm 0.012$
0.15 – 0.20	0.173	8.2	$-0.061 \pm 0.014 \pm 0.009$	$-0.092 \pm 0.021 \pm 0.012$	$-0.060 \pm 0.014 \pm 0.009$
0.20 – 0.30	0.242	9.8	$-0.042 \pm 0.011 \pm 0.007$	$-0.112 \pm 0.028 \pm 0.020$	$-0.043 \pm 0.011 \pm 0.007$
0.30 – 0.40	0.342	11.7	$-0.017 \pm 0.011 \pm 0.005$	$-0.068 \pm 0.065 \pm 0.025$	$-0.018 \pm 0.013 \pm 0.005$
0.40 – 0.50	0.441	13.3	$-0.007 \pm 0.011 \pm 0.002$	$-0.003 \pm 0.142 \pm 0.022$	$-0.009 \pm 0.014 \pm 0.003$
0.50 – 0.70	0.564	15.0	$0.003 \pm 0.008 \pm 0.001$	$0.100 \pm 0.294 \pm 0.039$	$0.005 \pm 0.012 \pm 0.002$